

# Generalized Adaptive Delayed Resonator Design for Complete Vibration Suppression With Force-Tuning Inaccuracies

Yifan Liu  and Li Cheng 

**Abstract**—Delayed resonator (DR) is an active vibration absorber that can enable complete vibration suppression through proper tuning of the actuation forces based on delayed (past) system states. However, the tuning requires exact knowledge of system parameters, thus causing residual vibrations which are sensitive to parametric inaccuracies/uncertainties. To eliminate such residual vibrations, we generalize an adaptation strategy to online correct the parameters of a classical control law by equating the effects of the force output at the vibration frequency to the alteration of the absorber's stiffness and damping, thereby accommodating the inaccurate estimations in all parameters involved in the tuning process. Furthermore, the equivalent model also allows the resulting adaptive DR to compensate for the inaccurate realization of the control parameters arising from the inaccurate hardware parameters. Simulations and experiments both verify the effectiveness and the efficacy of the general adaptation strategy, which significantly reduces the accuracy requirement for system parameter identifications and modeling for tuning DRs to achieve complete vibration suppression, while maintaining the simplicity of the delayed control logic.

**Index Terms**—Active vibration absorber, adaptive correction, delayed resonator (DR), parametric inaccuracy.

## I. INTRODUCTION

**D**ELAYED resonator (DR) is an active vibration absorber, which was proposed in the early work of Olgac and Holm-Hansen [1] by introducing proper time delays into the control loop to completely suppress the vibrations at a given frequency. Compared with the nondelayed control logic, e.g., the PD control [2], the DR models inevitable loop delays thus yielding more complete vibration suppression. Besides, manipulating delays can directly alter the phase of the system states collected for generating the actuation force without increasing control

terms, so the DR scheme can be achieved by only incorporating displacement [1], velocity [3], or acceleration [4] to simplify sensor implementation or enhance control robustness. The DR, through harnessing delay as a control parameter, has made itself a typical counter-intuitive example that a larger delay can enhance system performance. The patent [5] gave various engineering applications of the DR, e.g., vibration control of the helicopter fuselage, the gearbox, and the machining chatter.

DRs have been widely investigated. For instance, Sun and Xu [6] identified the loop delay, which was then tuned to enhance vibration suppression. Zhang et al. [7] modeled the friction effects. To reduce the effects of the measurement noise, Pilbauer et al. [8] and Kučera et al. [9] reported a distributed-delayed control logic to process all absorber states within a designated past time interval. Liu et al. [10] later evaluated the effects of the loop delay on this control logic, showing that the loop delay, albeit small, can result in no vibration suppression. Besides, Eris et al. [11] expedited system responses by actuating a DR with both nondelayed and delayed control terms. Yan et al. [12] and Wu et al. [13] enhanced active vehicle suspensions by optimizing the delayed control. Wang et al. [14] and Mohanty et al. [15] deployed DRs to settle nonlinear primary structures, see also [16]. Vyhřídál et al. [17] compared the tuning, stability, and energy issues of the DR subsystem when incorporating different absorber states. Cai et al. [18] further established a tuning framework using fractional-order operators. Meanwhile, the DR concept has also been extended to multiple-degree-of-freedom (MDOF) structures, yielding the so-called noncollected complete vibration suppression [19], [20], [21] to simultaneously confine the vibrations on the primary structure and the absorber. Moreover, Šika et al. [22] realized complete vibration suppression in multiple directions for robotic applications. In addition to complete vibration suppression, the strength of the delayed control is also reflected in various vibration control setups to enhance vibration reduction [23], [24], [25], [26].

Tuning a DR for complete vibration suppression requires two sets of parametric information: 1) parameters of the absorber substructure; and 2) vibration frequency. These parameters are usually regarded as perfectly known in existing works. However, in many practical applications, their a priori exact knowledge may not be available, or they may change during operation without being noticed, thus yielding inaccurately tuned

Received 17 July 2025; revised 12 October 2025; accepted 31 October 2025. Date of publication 15 December 2025; date of current version 11 March 2026. (Corresponding author: Li Cheng.)

The authors are with the Department of Mechanical Engineering, The Hong Kong Polytechnic University, Hong Kong, China (e-mail: yifan23.liu@connect.polyu.hk; li.cheng@polyu.edu.hk).

Digital Object Identifier 10.1109/TIE.2025.3632559

control parameters leading to residual vibrations. To tackle the problem, Pilbauer et al. [27] used a polynomial-distributed-delayed control law to handle the mismatch between the actual vibration frequency and its detection. In this case, DR allowed small residual vibrations within a small frequency band around the tuning frequency rather than achieving complete vibration suppression at that frequency, aiming to lower the sensitivity of residual vibrations. Later, Kuře et al. [28] assigned multiplicity to the imaginary roots of the DR subsystem, which lowered the sensitivity without affecting the complete vibration suppression at the tuning frequency. However, additional control forces need to be independently exerted on the primary to cope with the more severe stability issues. Note that the efforts in [27] and [28] are “indirect” solutions as they do not address the essential parametric mismatch, but rather reduce the resulting residual vibrations, see also [29], [30] for the DRs with a lever or a hybrid control law.

The direct solution to the problem of interest to eliminate the residual vibrations caused by parametric mismatch or inaccuracy dates back to 1999 when Renzulli et al. [31] first pointed out that the stiffness and damping of an absorber could undergo variations. The resulting mismatch between the real and nominal values of these structural parameters can yield an inaccurately tuned DR and subsequently residual vibrations. To address this, a gradient-based adaptive correction method for the control parameters of the DR prototype [3], including a gain plus a delay, was proposed under the prerequisite that the mismatch should yield limited deviations of the effective tuned pair from the theoretical one. Hosek and Olgac [32] later broke the small-deviation limitation by proposing a single-step correction method, which online identified the real values of the absorber’s stiffness and damping based on system responses. Notably, different from [27], [28], [29], [30], the solutions in [32] and [31] are adaptive and do not alter the control laws and system structure, thus simplifying implementation.

From the above, we notice that existing works only deal with the mismatch or inaccuracies in partial nominal parameters required for tuning, e.g., the frequency mismatch [27], [28], [29], [30] and deviations of absorber stiffness and damping [31], [32]. To further enhance the robustness of the DR, this work considers a more general case where all nominal parameters involved in the DR tuning are assumed inaccurate *a priori*, including the vibration frequency, absorber mass, stiffness, and damping, with the final task of eliminating residual vibrations. The idea follows [31], [32] to correct the control parameters of the DR prototype [3], rather than designing an advanced control law, in order to maintain the simplicity of the DR scheme. The method generalizes the single-step method reported in [32], given the core finding that the effects of all parametric inaccuracies on deviating the tuned actuation force can be equated to an imperfect alteration of the absorber’s stiffness and damping. Based on the equivalent model, we show that the resulting adaptive DR can additionally cope with the mismatch between the real output of the actuation force and the one designed in the controller, a less-exploited but important topic related to hardware performance. Furthermore, the previous work [32], which only handled the inaccuracies in the absorber’s stiffness

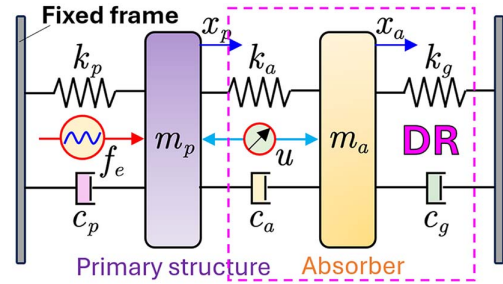


Fig. 1. Operating mode of the DR under investigation to settle the vibration of a force-excited primary structure.

and damping, requires the number of equations to be equal to the number of inaccurate parameters to be identified. This work breaks this limitation by conducting the adaptive correction without identifying the real system parameters, so the adaptive DR can be expected to fit more complex or general applications.

In the following, Section II introduces the DR concept. Section III summarizes the previous work [32] and the general adaptive problem to be handled. Section IV introduces the design procedure of the adaptive correction strategy. Section V numerically and experimentally verifies the effectiveness of the adaptive DR. Main conclusion is drawn in Section VI.

## II. PRELIMINARIES

The operating mode of the DR under investigation is shown in Fig. 1. The primary structure is harmonically excited by a force  $f_e$ , and  $u$  is an actuation force following a delayed control law to achieve active vibration suppression. The task of the DR is to achieve  $|x_p| \equiv 0$  when  $|f_e| \neq 0$  by tuning  $u$ , yielding the so-called complete vibration suppression.

We point out that the considered model is built upon the one in [32] by adding grounded components ( $k_g, c_g$ ) to the DR, aiming to show that our generalized adaptive DR design, to be introduced later, can handle more inaccurate parameters involved in the force tuning. Note that in the given context of complete vibration suppression, the primary does not have to be SDOF to conduct the force tuning and adaptation. To avoid interrupting the flow of how this work evolves from [32], we briefly discuss an MDOF case in Appendix B as an extension to test the applicability of our results.

### A. Dynamical Modeling

The dynamics of the 2DOF coupled system follows:

$$\begin{cases} m_a \ddot{x}_a + c_g \dot{x}_a + k_g x_a + c_a (\dot{x}_a - \dot{x}_p) + k_a (x_a - x_p) = u \\ m_p \ddot{x}_p + c_p \dot{x}_p + k_p x_p + c_a (\dot{x}_p - \dot{x}_a) + k_a (x_p - x_a) = f_e - u \end{cases} \quad (1)$$

where  $x(\cdot)$ ,  $m(\cdot)$ ,  $c(\cdot)$ , and  $k(\cdot)$  represent absolute displacement, mass, damping, and stiffness, respectively;  $(x_a, x_p, u, f_e)$  are functions of the physical time denoted as  $t$ . Following the DR prototype [1], the delayed control law simply follows:

$$u(t) = g x_a(t - \tau) \quad (2)$$

where  $g$  is the gain and  $\tau$  is a time delay, which are the two control parameters. Substituting (2) into (1) and applying Laplace transform lead to

$$\begin{bmatrix} z_{11} & z_{12} \\ z_{21} & z_{22} \end{bmatrix} \begin{bmatrix} X_a \\ X_p \end{bmatrix} = \begin{bmatrix} 0 \\ F_e \end{bmatrix} \quad (3)$$

where  $X_a = \mathcal{L}(x_a)$ ,  $X_p = \mathcal{L}(x_p)$ , and  $F_e = \mathcal{L}(f_e)$ , in which  $\mathcal{L}(\cdot)$  denotes the Laplace transform. Besides, one has

$$\begin{cases} z_{11} = m_a s^2 + (c_a + c_g) s + k_a + k_g - g e^{-\tau s} \\ z_{12} = -(c_a s + k_a) \\ z_{21} = -(c_a s + k_a) + g e^{-\tau s} \\ z_{22} = m_p s^2 + (c_p + c_a) s + k_p + k_a \end{cases} \quad (4)$$

where  $s$  is the Laplace variable. The active force  $u$  makes sense only if the system is stable, i.e., the characteristic equation

$$CE(s, g, \tau) = z_{11} z_{22} - z_{12} z_{21} = 0 \quad (5)$$

has all its characteristic roots on the left half of the complex plane. When  $\tau \neq 0$ , equation (5) has infinite characteristic roots, the distribution of which is numerically checked by the Quasi-polynomial root-finder (QPMR) algorithm [33] in this work.

### B. Tuning Rules of $(g, \tau)$ for Complete Vibration Suppression

Substituting the condition for complete vibration suppression, i.e.,  $|x_p| \equiv 0$ , into the first equation of (1) yields

$$u(t) = m_a \ddot{x}_a + (c_a + c_g) \dot{x}_a + (k_a + k_g) x_a \quad (6)$$

which depicts the SDOF absorber dynamics, where the frequency of  $x_a$  concurs with that of the excitation  $f_e$ . Equation (6) gives the necessary condition for tuning  $u$ . With the control law (2), the Laplace transform of (6) is

$$(m_a s^2 + (c_a + c_g) s + k_a + k_g) - g e^{-\tau s} = 0. \quad (7)$$

Substituting  $s = j\omega$ , in which  $j = \sqrt{-1}$ , and  $\omega$  is the frequency of  $f_e$ , into (7) and balancing the real and imaginary parts of the resulting complex equation yield the tuned pair of  $(g, \tau)$  denoted as

$$*u_t \rightarrow \begin{cases} *g_t(\omega) = \pm \sqrt{(k_a + k_g - m_a \omega^2)^2 + [(c_a + c_g)\omega]^2} \\ *\tau_{t,b}(\omega) = \frac{1}{\omega} \left[ \text{atan2} \left( \frac{-(c_a + c_g)\omega}{k_a + k_g - m_a \omega^2} \right) + 2\pi(b-1) + \rho\pi \right] \end{cases} \quad (8)$$

where the subscript  $(\cdot)_t$  means ‘‘tuned,’’  $b \in \mathbb{Z}^+$  denotes the branch number, the mechanism of which is left to [1] and [17];  $\rho = 0$  and  $\rho = 1$  correspond to  $*g_t > 0$  and  $*g_t < 0$ , respectively. Note from (8) that only the structural parameters of the absorber, i.e.,  $(m_a, k_a, k_g, c_a, c_g)$ , are needed to determine the desired tuned active force  $*u_t$ , in addition to the excitation frequency  $\omega$ .

### III. ADAPTATION PROBLEM: REVIEW AND GENERALIZATION

From (8), residual vibrations can appear due to the inaccurate knowledge of  $(\omega, m_a, k_a, k_g, c_a, c_g)$ . This section first reviews the existing means for handling this problem, serving as a reference for subsequent analyses, and then introduces the more general case to be tackled in this work. To facilitate discussions, the following symbolic definitions are used.

*Definition 1:* Real system parameters or effective values are denoted as  $(\omega, m_a, k_a, k_g, c_a, c_g, g, \tau)$ . Nominal values of such parameters are denoted as  $(\hat{\omega}, \hat{m}_a, \hat{k}_a, \hat{k}_g, \hat{c}_a, \hat{c}_g, \hat{g}, \hat{\tau})$ .  $\square$

*Definition 2:* Real and nominal actuation forces are denoted by  $u$  and  $\hat{u}$ , respectively. That is,  $u$  and  $\hat{u}$  correspond to  $(g, \tau)$  and  $(\hat{g}, \hat{\tau})$ , respectively. Note that  $u \neq \hat{u}$  is allowed in this work, as to be demonstrated. Besides, the nominal tuned force  $\hat{u}_t$  corresponds to  $(\hat{g}_t, \hat{\tau}_t)$ , which are the tuned pair resulting from substituting  $(\hat{\omega}, \hat{m}_a, \hat{k}_a, \hat{k}_g, \hat{c}_a, \hat{c}_g)$  into (8).  $\square$

#### A. Review of the Single-Step Adaptation Method

When  $(k_g, \tau_g) = (0, 0)$ , Hosek and Olgac [32] proposed a single-step adaptation method to handle the case where only the knowledge of  $(k_a, c_a)$  is inaccurate, i.e.,  $(\hat{k}_a, \hat{c}_a) \neq (k_a, c_a)$ . The method is based on the transfer function from  $x_a$  to  $x_p$

$$G_a^p(s) = \frac{X_p}{X_a} = \frac{m_a s^2 + (c_a + c_g) s + (k_a + k_g) - g e^{-\tau s}}{c_a s + k_a} \quad (9)$$

which can be obtained by applying the Laplace transform to the first equation of (1). Substituting  $s = j\omega$  into (9) leads to

$$G_a^p(j\omega) = \frac{k_a + k_g - m_a \omega^2 + j(c_a + c_g)\omega - g e^{-j\tau\omega}}{k_a + j c_a \omega} \quad (10)$$

Comparing the forms of (7) and (10), one can find that  $G_a^p(j\omega) = 0$  holds in the ideal case where  $(g, \tau) = (\hat{g}_t, \hat{\tau}_t) = (*g_t, *\tau_t)$ . If  $(\hat{k}_a, \hat{c}_a)$  are inaccurate,  $(\hat{g}_t, \hat{\tau}_t) \neq (*g_t, *\tau_t)$ , and thus  $G_a^p(j\omega) \neq 0$ , so resulting in residual vibrations  $|x_p| \neq 0$ . In this case, we reconstruct (10) based on the actual responses of  $(x_p, x_a)$ , leading to

$$\tilde{G}_a^p(j\omega) = \frac{k_a + k_g - m_a \omega^2 + j(c_a + c_g)\omega - \hat{g}_t e^{-j\hat{\tau}_t \omega}}{k_a + j c_a \omega} \quad (11)$$

in which  $\tilde{G}_a^p(j\omega)$  is a complex value, and  $(\hat{g}_t, \hat{\tau}_t)$  are known but inaccurate. Taking  $(k_a, c_a)$  in (11) as two variables, balancing the real and imaginary parts on the two sides of (11) yields two algebraic equations so the exact values  $(k_a, c_a)$  can be obtained. Then, the desired condition  $(\hat{g}_t, \hat{\tau}_t) = (*g_t, *\tau_t)$  can be achieved by performing another tuning mechanism (8) after correcting  $(\hat{k}_a, \hat{c}_a)$  to the obtained  $(k_a, c_a)$ , thus eliminating residual vibrations and completing the single-step adaptation.

#### B. General Adaptation Problem

Since the single-step correction method needs to solve the complex equation (11), it can only handle the inaccuracies in

two variables requiring all the other variables to be known, i.e., nominal values concur with the real (actual) ones. As a further step, we handle the general case where the knowledge of all variables in (11) can be inaccurate. The said inaccuracies can stem from two aspects.

- 1)  $(\hat{\omega}, \hat{m}_a, \hat{k}_a, \hat{k}_g, \hat{c}_a, \hat{c}_g) \neq (\omega, m_a, k_a, k_g, c_a, c_g)$ . This case indicates that errors exist in identifying or measuring the vibration frequency and the parameters of the absorber substructure, or their variations are not detected.
- 2)  $(\hat{g}, \hat{\tau}) \neq (g, \tau)$ . It means that a mismatch exists between the nominal and the real force output, which can be attributed to the uncalibrated actuators and inherent loop delays. That is, even if  $(\hat{g}_t, \hat{\tau}_t) = (g_t^*, \tau_t^*)$ , one has  $u_t \neq u_t^*$ .

Note that the involved variables cover all parameters needed for tuning  $u$ , so the solution to the adaptation problem can lower the requirement for system identification and measurements, thus extending the applicability of the DR in practice.

*Remark 1:* Different from the single-step method, the considered adaptation problem does not identify the real system parameters. Since we can alter system dynamics only by manipulating  $(\hat{g}, \hat{\tau})$  in the control loop, the task is to correct the nominal tuned pair  $(\hat{g}_t, \hat{\tau}_t)$  to eliminate or neutralize the effects of the parametric inaccuracies on complete vibration suppression. Besides, the inaccuracy by itself means that the differences between the nominal and the real values, if they exist, are small, so system stability still holds, and the consequences are residual rather than amplified vibrations.  $\square$

*Remark 2:* The problem lies in that one does not exactly know all the required parameters of a determinative system when tuning the DR. That is, during the following correction process, although  $(\omega, m_a, k_a, k_g, c_a, c_g)$  are (partly) unknown, they are constant or vary sufficiently slowly making the effect of the transient process negligible. In case b) defined above, although  $(g, \tau) \neq (\hat{g}, \hat{\tau})$ , the relationship governing the differences between such two pairs is linear and fixed (e.g., constant scaling, shifting, or the combination). The above guarantees the linearity, causality, and controllability of the complete vibration suppression and the adaptation.  $\square$

#### IV. ADAPTIVE CORRECTION STRATEGY

The proposed adaptive correction strategy generalizes the single-step method and is still based on the transfer function (10), therefore requiring the online monitoring of the system responses  $(x_a, x_p)$ .

##### A. Effects of the Tuned Force $u_t$ and Equivalent Model

Revisiting (7) or the numerator of the right-hand-side term of (10), to achieve  $|x_p| \equiv 0$ , it necessitates that

$$\begin{cases} (k_a + k_g - m_a \omega^2) - k_u = 0 \\ (c_a + c_g) \omega + c_u = 0 \end{cases} \quad \begin{cases} k_u = g \cos(\tau \omega) \\ c_u = g \sin(\tau \omega) \end{cases} \quad (12)$$

which holds only when  $(g, \tau) = (g_t^*, \tau_t^*)$ . That is, the ideally tuned force  $u_t^*$  for complete vibration suppression can be regarded as an alternation of the equivalent stiffness and damping

of the absorber at  $\omega$ , i.e.,  $c_u$  eliminates the damping effect, and  $k_u$  moves the equivalent natural frequency of the absorber to  $\omega$  by having  $\sqrt{(k_a + k_g - k_u)/m_a} = \omega$ . When actually achieving  $\hat{u}_t$  as  $u_t$ , i.e.,  $(\hat{g}_t, \hat{\tau}_t)$  are achieved as  $(g_t, \tau_t)$ , we can conclude from the inverse of (12) that

$$\begin{cases} g_t \cos(\tau_t \hat{\omega}) = \alpha_1 \hat{g}_t \cos(\hat{\tau}_t \hat{\omega}) = \alpha_1 (\hat{k}_a + \hat{k}_g - \hat{m}_a \hat{\omega}^2) \\ g_t \sin(\tau_t \hat{\omega}) = \beta_1 \hat{g}_t \sin(\hat{\tau}_t \hat{\omega}) = \beta_1 ((\hat{c}_a + \hat{c}_g) \hat{\omega}) \end{cases} \quad (13)$$

where  $(\alpha_1, \beta_1) \in \mathbb{R}^2$  signify the inaccurate realization of  $(\hat{g}_t, \hat{\tau}_t)$  as per case b) in Section III-B. Clearly, if  $(\alpha_1, \beta_1) \neq (1, 1)$ ,  $u_t$  deviates from  $\hat{u}_t$ . We next incorporate the inaccuracies of  $(\hat{\omega}, \hat{m}_a, \hat{k}_g, \hat{c}_g)$  into  $(\hat{k}_a, \hat{c}_a)$  by enforcing

$$\begin{cases} g_t \cos(\tau_t \omega) = \alpha_2 \hat{k}_a + k_g - m_a \omega^2 \\ g_t \sin(\tau_t \omega) = -(\beta_2 \hat{c}_a + c_g) \omega \end{cases} \quad (14)$$

where  $(\alpha_2, \beta_2) \in \mathbb{R}^2$  are two balancing coefficients, and  $(\alpha_2, \beta_2) \neq (\alpha_1, \beta_1)$ . From the perspective of (14), when actually achieving  $\hat{u}_t$ , or equivalently,  $(\hat{g}_t, \hat{\tau}_t)$ , we “mathematically” reduce the general case where  $(\hat{\omega}, \hat{g}_t, \hat{\tau}_t, \hat{m}_a, \hat{k}_a, \hat{k}_g, \hat{c}_a, \hat{c}_g)$  are inaccurate into the case where only the knowledge of the absorber stiffness and damping respectively governed by  $\alpha_2 \hat{k}_a$  and  $\beta_2 \hat{c}_a$  are inaccurate. In this case, if  $(\alpha_2 \hat{k}_a, \beta_2 \hat{c}_a) \neq (k_a, c_a)$ , the real force output  $u_t$  governed by  $(g_t, \tau_t)$  cannot achieve the desired alternation of the equivalent stiffness and damping of the real absorber, so residual vibrations appear.

##### B. Correction Strategy

Based on the equivalent model (14) for actually achieving  $\hat{u}_t$  as  $u_t$ , we substitute  $(g, \tau) = (g_t, \tau_t)$  into (10), yielding

$$\begin{aligned} \tilde{G}_a^p(j\omega) &= \frac{k_a + k_g - m_a \omega^2 + j(c_a + c_g)\omega - g_t [\cos(\tau_t \omega) - j \sin(\tau_t \omega)]}{k_a + j c_a \omega} \\ &= \frac{\Delta k_a + j \Delta c_a \omega}{k_a + j c_a \omega} = \frac{\Delta k_a + j \Delta c_a \omega}{\Delta k_a + \alpha_2 \hat{k}_a + j(\Delta c_a + \beta_2 \hat{c}_a) \omega} \end{aligned} \quad (15)$$

where  $\tilde{G}_a^p(j\omega)$  is real-time constructed as per the actual responses  $(x_p, x_a)$ , and

$$\begin{cases} \Delta k_a = k_a - \alpha_2 \hat{k}_a \\ \Delta c_a = c_a - \beta_2 \hat{c}_a \end{cases} \quad (16)$$

which are the errors of altering the equivalent stiffness and damping. Note that the right-hand-side terms in (15) govern the actual frequency responses when the actuation force is tuned according to the nominal values  $(\hat{\omega}, \hat{m}_a, \hat{k}_a, \hat{k}_g, \hat{c}_a, \hat{c}_g)$  while taking into account the inaccurate realization of  $(\hat{g}_t, \hat{\tau}_t)$ . Besides, the desired complete vibration suppression  $|x_p| = 0$  corresponds to

$$\begin{cases} |\tilde{G}_a^p(j\omega)| = 0, \text{ or} \\ (\Delta k_a, \Delta c_a) = (0, 0) \end{cases} \quad (17)$$

in which the former condition is the causal result of the latter one. Since (15) is indeterminate (i.e., the number of variables exceeds that of the equations), to achieve  $(\Delta k_a, \Delta c_a) = (0, 0)$ , we update the nominal values  $(\hat{k}_a, \hat{c}_a)$  following:

$$\begin{cases} \hat{k}_a^{(n)} = \hat{k}_a^{(n-1)} + \Delta \hat{k}_a^{(n)} \\ \hat{c}_a^{(n)} = \hat{c}_a^{(n-1)} + \Delta \hat{c}_a^{(n)} \end{cases} \quad (18)$$

where  $(\cdot)^{(n)}$  denotes the  $n^{\text{th}}$  updating step, and the to-be-designed step  $(\Delta \hat{k}_a^{(n)}, \Delta \hat{c}_a^{(n)})$  must satisfy

$$\lim_{n \rightarrow \infty} (\Delta \hat{k}_a^{(n)}, \Delta \hat{c}_a^{(n)}) = (\Delta k_a, \Delta c_a) = (0, 0) \quad (19)$$

in which  $(\Delta k_a, \Delta c_a)$  are defined in (16). In this process,  $(\hat{g}_t, \hat{\tau}_t)$  at each step are corrected in the controller as

$$\hat{u}_t^{(n)} \rightarrow \begin{cases} \hat{g}_t^{(n)} (\hat{k}_a^{(n)}, \hat{c}_a^{(n)}) \\ = \pm \sqrt{(\hat{k}_a^{(n)} + \hat{k}_g - \hat{m}_a \hat{\omega}^2)^2 + [(\hat{c}_a^{(n)} + \hat{c}_g) \hat{\omega}]^2} \\ \hat{\tau}_{t,b}^{(n)} (\hat{k}_a^{(n)}, \hat{c}_a^{(n)}) \\ = \frac{1}{\hat{\omega}} \left[ a \tan 2 \left( \frac{-(\hat{c}_a^{(n)} + \hat{c}_g) \hat{\omega}}{\hat{k}_a^{(n)} + \hat{k}_g - \hat{m}_a \hat{\omega}^2} \right) + 2\pi(b-1) + \rho\pi \right] \end{cases} \quad (20)$$

where  $(\hat{k}_a^{(0)}, \hat{c}_a^{(0)}) = (\hat{k}_a, \hat{c}_a)$  are used for initial values, and nominal values  $(\hat{\omega}, \hat{m}_a, \hat{k}_g, \hat{c}_g)$  are fixed in the correction process. If  $(\Delta \hat{k}_a^{(1)}, \Delta \hat{c}_a^{(1)}) = (\Delta k_a, \Delta c_a)$ , i.e.,  $\alpha_2 = \beta_2 = 1$ , we retreat to the reduced case of the single-step correction method. When recursively executing (15), (16), (18) and (20), equation (14) has the generalized form of

$$\begin{cases} g_t^{(n)} \cos(\tau_t^{(n)} \omega) = \alpha_2^{(n)} (\hat{k}_a^{(n-1)} + \Delta \hat{k}_a^{(n)}) + k_g - m_a \omega^2 \\ = \alpha_2^{(n)} [k_a + (1 - \alpha_2^{(n-1)}) \hat{k}_a^{(n-1)}] + k_g - m_a \omega^2 \\ g_t^{(n)} \sin(\tau_t^{(n)} \omega) = [\beta_2^{(n)} (\hat{c}_a^{(n-1)} + \Delta \hat{c}_a^{(n)}) + c_g] \omega \\ = [\beta_2^{(n)} (c_a + (1 - \beta_2^{(n-1)}) \hat{c}_a^{(n-1)}) + c_g] \omega. \end{cases} \quad (21)$$

Under the prerequisite (19), implying that each correction transfers the effects of the nonzero  $(\Delta \hat{k}_a^{(n)}, \Delta \hat{c}_a^{(n)})$  to  $(g_t^{(n)}, \tau_t^{(n)})$ , we have  $(|\alpha_2^{(n)}|, |\beta_2^{(n)}|) \rightarrow (1, 1)$  as  $n$  increases, i.e.,  $(g_t^{(n)}, \tau_t^{(n)})$  governing the real force output  $u_t$  converge to the desired pair  $(g_t^*, \tau_t^*)$  as per (21), thus eliminating residual vibrations. The updating step  $(\Delta \hat{k}_a^{(n)}, \Delta \hat{c}_a^{(n)})$  is determined next.

*Remark 3:* Since the recursive correction process (20) is based on the equivalent model (14) of  $u_t$ , the final convergence  $(|\alpha_2^{(n)}|, |\beta_2^{(n)}|) \rightarrow (1, 1)$  or  $(\Delta \hat{k}_a, \Delta \hat{c}_a) = (0, 0)$ , does not yield  $(\hat{k}_a^{(n)}, \hat{c}_a^{(n)}) = (k_a, c_a)$  since  $(\hat{k}_a^{(n)}, \hat{c}_a^{(n)})$  now also

take into account the inaccuracies of  $(\hat{\omega}, \hat{m}_a, \hat{k}_g, \hat{c}_g)$  and in achieving  $(\hat{g}_t, \hat{\tau}_t)$ , see also Remark 1.  $\square$

*Remark 4:* Incorporating the inaccuracies of all nominal values in (14) into  $(\hat{k}_a, \hat{c}_a)$  is reasonable given the form of (15). If we replace  $(\hat{k}_a, \hat{c}_a)$  with  $(\hat{\omega}, \hat{m}_a, \hat{k}_g, \hat{c}_g)$ , the number of variables of the denominator on the right side of (15) will be increased, thus complicating the correction process.  $\square$

### C. Updating Step

To achieve the correction process (20), we need to determine  $(\Delta \hat{k}_a^{(n)}, \Delta \hat{c}_a^{(n)})$  in (18) under the prerequisite (19). Note that  $(\Delta \hat{k}_a^{(n)}, \Delta \hat{c}_a^{(n)})$  are the approximations of  $(\Delta k_a, \Delta c_a)$ . Let us then start with investigating the form of  $(\Delta k_a, \Delta c_a)$ . Letting

$$\tilde{G}_a^p(j\omega) = \frac{\mathcal{F}(\mathbf{x}_p(t))}{\mathcal{F}(\mathbf{x}_a(t))} = \sigma + j\varphi \quad (22)$$

where  $\mathcal{F}(\cdot)$  denotes the Fourier transform,  $(\sigma, \varphi) \in \mathbb{R}^2$ , and  $(\mathbf{x}_p, \mathbf{x}_a)$  denote the time-domain datasets of  $(x_p, x_a)$ , we can solve  $(\Delta k_a, \Delta c_a)$  from (15) as

$$\begin{cases} \Delta k_a = -\frac{\alpha_2 \hat{k}_a (\sigma^2 + \varphi^2) + \beta_2 \omega \varphi \hat{c}_a - \alpha_2 \sigma \hat{k}_a}{\sigma^2 + \varphi^2 - 2\sigma + 1} \\ \Delta c_a = \frac{-\beta_2 \hat{c}_a \omega (\sigma^2 + \varphi^2) + \beta_2 \omega \sigma \hat{c}_a + \alpha_2 \varphi \hat{k}_a}{(\sigma^2 + \varphi^2 - 2\sigma + 1) \omega} \end{cases} \quad (23)$$

in which the exact values of  $(\alpha_2, \beta_2, \omega)$  are unknown. Next, we reconstruct  $(\Delta k_a, \Delta c_a)$  as

$$\begin{cases} \Delta k_a = \Delta k_{a,M} + O_k(\alpha_2, \beta_2, \omega) \\ \Delta c_a = \eta [\Delta c_{a,M} + O_c(\alpha_2, \beta_2, \omega)] \end{cases} \quad (24)$$

where  $\eta = \hat{\omega}/\omega \approx 1$ , and  $(\Delta k_{a,M}, \Delta c_{a,M})$  are defined as main terms, which are independent of  $(\alpha_2, \beta_2, \omega)$ , satisfying

$$\begin{cases} \Delta k_{a,M} = -\frac{\hat{k}_a (\sigma^2 + \varphi^2) + \varphi \hat{c}_a \hat{\omega} - \sigma \hat{k}_a}{\sigma^2 + \varphi^2 - 2\sigma + 1} \\ \Delta c_{a,M} = \frac{-\hat{c}_a \hat{\omega} (\sigma^2 + \varphi^2) + \sigma \hat{c}_a \hat{\omega} + \varphi \hat{k}_a}{(\sigma^2 + \varphi^2 - 2\sigma + 1) \hat{\omega}}. \end{cases} \quad (25)$$

Besides, the remainders  $(O_k, O_c)$  in (24) are functions of  $(\alpha_2, \beta_2, \omega)$  following:

$$\begin{cases} O_k(\alpha_2, \beta_2, \omega) = -\frac{\hat{k}_a (\sigma^2 + \varphi^2) (\alpha_2 - 1) + \varphi \hat{c}_a (\beta_2 \omega - \hat{\omega}) - \sigma \hat{k}_a (\alpha_2 - 1)}{\sigma^2 + \varphi^2 - 2\sigma + 1} \\ O_c(\alpha_2, \beta_2, \omega) = \frac{-\hat{c}_a (\sigma^2 + \varphi^2) (\beta_2 \omega - \hat{\omega}) + \sigma \hat{c}_a (\beta_2 \omega - \hat{\omega}) + \varphi \hat{k}_a (\alpha_2 - 1)}{(\sigma^2 + \varphi^2 - 2\sigma + 1) \hat{\omega}}. \end{cases} \quad (26)$$

When  $|\tilde{G}_a^p(j\omega)| = 0$ , i.e.,  $(\sigma, \varphi) \rightarrow (0, 0)$ , the main terms  $(\Delta k_{a,M}, \Delta c_{a,M})$  dictate the values of  $(\Delta k_a, \Delta c_a)$  given that

$$\begin{cases} \lim_{\sigma \rightarrow 0} O_k(\alpha_2, \beta_2, \omega) \rightarrow 0 \\ \lim_{\varphi \rightarrow 0} \frac{\Delta k_{a,M}}{O_k(\alpha_2, \beta_2, \omega)} \Big|_{\sigma \rightarrow 0} \rightarrow 0 \\ \lim_{\sigma \rightarrow 0} O_c(\alpha_2, \beta_2, \omega) \Big|_{\varphi \rightarrow 0} \rightarrow 0 \\ \lim_{\varphi \rightarrow 0} \frac{\Delta c_{a,M}}{O_c(\alpha_2, \beta_2, \omega)} \Big|_{\sigma \rightarrow 0} \rightarrow 0. \end{cases} \quad (27)$$

Hence, in the correction process (18) and (20) to eliminate residual vibrations governed by  $|\tilde{G}_a^p(j\omega)| = |x_p|/|x_a| \approx 0_+$ , we have  $(\Delta k_{a,M}, \Delta c_{a,M}) \gg (O_k, O_c)$ . Also, since the effects of enforcing  $\eta = 1$  in (24) can be incorporated into  $\beta_2$  of (16) similar to (14) and since  $\eta$  takes no effect when  $\Delta c_a \rightarrow 0$ , we design  $(\Delta \hat{k}_a^{(n)}, \Delta \hat{c}_a^{(n)})$  as per main terms (25), yielding

$$\begin{cases} \Delta \hat{k}_a^{(n)} = -\frac{\hat{k}_a^{(n-1)}[(\sigma^{(n)})^2 + (\varphi^{(n)})^2] + \varphi^{(n)} \hat{c}_a^{(n-1)} \hat{\omega} - \sigma^{(n)} \hat{k}_a^{(n-1)}}{(\sigma^{(n)})^2 + (\varphi^{(n)})^2 - 2\sigma^{(n)} + 1} \\ \Delta \hat{c}_a^{(n)} = -\frac{\hat{c}_a^{(n-1)} \hat{\omega}[(\sigma^{(n)})^2 + (\varphi^{(n)})^2] + \sigma^{(n)} \hat{c}_a^{(n-1)} \hat{\omega} + \varphi^{(n)} \hat{k}_a^{(n-1)}}{[(\sigma^{(n)})^2 + (\varphi^{(n)})^2 - 2\sigma^{(n)} + 1] \hat{\omega}} \end{cases} \quad (28)$$

in which all variables are known. Clearly, the remainders  $(O_k, O_c)$  ignored in (28) should impose no significant effects on the differences between  $(\hat{g}_t^{(n)}, \hat{\tau}_t^{(n)})$  and  $(\hat{g}_t^{(n-1)}, \hat{\tau}_t^{(n-1)})$  so residual vibrations can be reduced as  $n$  increases.

Note also from (27) that  $(O_k, O_c) \rightarrow (0, 0)$  as  $|x_p|/|x_a| \rightarrow 0$ . Therefore, the effects of  $(O_k, O_c)$  do not affect the arrival at the final convergence to  $|x_p| \equiv 0$ . That is,  $|x_p| \equiv 0$  and  $(O_k, O_c) = (0, 0)$  are achieved simultaneously, satisfying the prerequisite (19). Now, by online activating the adaptive correction strategy governed by (18), (20), and (28), we can tune the DR to achieve  $|x_p| \equiv 0$  or  $(g_t, \tau_t) = (\hat{g}_t^*, \hat{\tau}_t^*)$  without needing to know the real values of  $(\omega, m_a, k_a, k_g, c_a, c_g)$  and the exact relationship between  $(\hat{g}_t, \hat{\tau}_t)$  and  $(g_t, \tau_t)$  to confront the general adaptation problem proposed in Section III-B.

*Remark 5:* Each correction step  $n$  assumes  $(O_k, O_c) = (0, 0)$ , i.e.,  $(\alpha_2, \beta_2\omega) = (1, \hat{\omega})$  as per (26). Combining with (15), it assumes that  $(\Delta \hat{k}_a^{(n)}, \Delta \hat{c}_a^{(n)}) = (\Delta k_a, \Delta c_a)$  exactly holds at each  $n$ . That is, the above recursive adaptation, with convergence proved, can be regarded as recursively executing single-step corrections to handle inaccurate  $(\hat{k}_a^{(n)}, \hat{c}_a^{(n)})$ .  $\square$

#### D. Complementary Conditions in Practical Context

Since the adaptation is based on the transfer function (9) or (15), which governs steady-state responses, every two consecutive correction steps should be separated by a certain time elapse [32], say  $T$ , for settling system dynamics and then collecting the data  $(x_p, x_a)$  to construct (22). We then let

$$T > t_s + t_{dc} \quad (29)$$

where  $t_s$  is the settling time of the coupled system and  $t_{dc}$  is the time taken for data collection of  $(x_p, x_a)$  in steady states. e.g., if we collect three cycles of data, then  $t_{dc} = 3/\hat{\omega}$ , with  $\hat{\omega}$  in Hz. For  $t_s$ , it can be estimated by the real part, say  $\sigma_{CE}$ , of the rightmost pair of characteristic roots of (4). Given that the transient responses being reduced by more than 98% can be represented as  $\exp(\sigma_{CE}t_s) < 2\%$ , we let  $t_s = -4/\sigma_{CE}$ , where  $\sigma_{CE} < 0$  must hold for a stable system.

Considering that the time-based criterion (29) to determine the steady state may be not robust enough in practical applications given possible perturbations. As an additional and direct insurance, one can check if

$$\text{RMSE}(\mathbf{x}_{p,N}, \mathbf{x}_{p,N-1}) \approx 0 \quad (30)$$

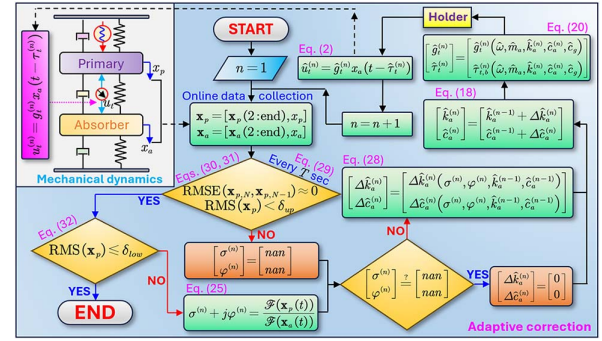


Fig. 2. Flow chart of the adaptive correction process. *nan* meaning “not a number” signifies that correction is inoperable.

where  $\text{RMSE}(\cdot)$  calculates the root mean square error, and  $\mathbf{x}_{p,N}$  and  $\mathbf{x}_{p,N-1}$  denote the datasets of  $x_p$  for the most recent cycle and the preceding one, respectively. Besides, to meet the condition  $|\tilde{G}_a^p(j\omega)| \approx 0_+$  in (28) before each step of executing the correction, we can check if

$$\text{rms}(\mathbf{x}_p) < \delta_{up} \quad (31)$$

in addition to (30), where  $\text{rms}(\cdot)$  calculates the root mean square,  $\delta_{up}$  is a user-defined threshold value, and  $\mathbf{x}_p$  is the dataset of  $x_p$  dynamically sampled over at least one past cycle. On the other hand, a lower threshold value should be set, i.e.,

$$\text{rms}(\mathbf{x}_p) > \delta_{low} \quad (32)$$

where  $0_+ < \delta_{low} \ll \delta_{up}$ , given that the measurement noise becomes dominant as  $|x_p| \rightarrow 0$ . Otherwise, the resulting errors in constructing  $(\sigma, \varphi)$  in (22) or  $(\hat{g}_t, \hat{\tau}_t)$  can amplify residual vibrations and even lead to destabilization.

*Remark 6:* By manipulating  $(T, \delta_{low})$  defined in (29) and (32), one can determine the rate and sensitivity of the correction, which together determine the computational resource consumption of the adaptive correction.  $\square$

#### E. Correction Flow

The main steps of the overall adaptive correction process are recapped in Fig. 2, where  $(\mathbf{x}_p, \mathbf{x}_a)$  have the same fixed length as per  $t_{dc}$ , and the operation Holder means maintaining the output  $(\hat{g}_t^{(n)}, \hat{\tau}_t^{(n)})$  until their values are changed. Remark 2 holds for a complete correction process from START to END.

## V. CASE STUDIES

Numerical and experimental tests are performed for demonstration. Particularly, the possible sources causing the inaccuracies/uncertainties in achieving the nominal values  $(\hat{g}, \hat{\tau})$  are discussed. When tuning  $(\hat{g}, \hat{\tau})$ , the positive gain and the smallest branch rendering a positive tuned delay are considered without loss of generality, so  $(\rho, b) = (0, 2)$ . The SIMULINK-based simulation models and video recordings of the experiments are available at Appendix C.

TABLE I  
REAL STRUCTURAL PARAMETERS OF THE COUPLED SYSTEM IN FIG. 1 AND THE NOMINAL  
VALUES OF THE ABSORBER SUBSTRUCTURE

	Mass [kg]	Stiffness [N/m]	Damping [Ns/m]
Primary structure	$m_p = 0.965$	$k_p = 1465$	$c_p = 5.0$
Absorber	$m_a = 0.51$	$(k_a, k_g) = (753, 11)$	$(c_a, c_g) = (4.3, 1.8)$
	$\hat{m}_a = 1.02m_a$	$(\hat{k}_a, \hat{k}_g) = (1.05k_a, 2k_g)$	$(\hat{c}_a, \hat{c}_g) = (0.92c_a, 1.06c_g)$

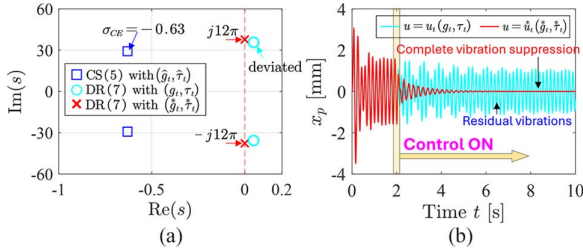


Fig. 3. (a) Spectra of the coupled system (4) and the DR subsystem (7) for different pairs of  $(g, \tau)$ . (b) Dynamics of  $x_p$  when the DR tuned with  $(g_t, \tau_t)$  and the desired pair  $(\hat{g}_t, \hat{\tau}_t)$  is activated at  $t = 2$  s.

### A. Numerical Simulation

1) *Parameter Settings*: In simulation, the real structural parameters of the coupled system in Fig. 1 are given in the first two rows of Table I, and the nominal values of the absorber, which deviate from the exact values for tuning the DR, are shown in the last row, where  $\hat{k}_g = 2k_g$  is considered given the small value of  $k_g$  compared with  $k_a$ . The corresponding experimental setup is to be introduced later. A harmonic excitation  $f_e$  of amplitude  $|f_e| = 4$  N at the frequency  $\omega = 6$  Hz is considered in the test. Equations (30) and (32) are not considered, given the ideal simulation environment.

Given the real values  $(\omega, m_a, k_a, k_g, c_a, c_g)$ , the desired tuned pair for complete vibration suppression can be obtained from (8) as  $(\hat{g}_t^*, \hat{\tau}_t^*) = (233.2 \text{ N/m}, 129.5 \text{ ms})$ . When tuning  $u$  as per the inaccurate nominal values  $(\hat{\omega}, \hat{m}_a, \hat{k}_a, \hat{k}_g, \hat{c}_a, \hat{c}_g)$ , where the excitation frequency is detected as  $\hat{\omega} = 0.98 \times \omega$ , we have  $(\hat{g}_t^{(0)}, \hat{\tau}_t^{(0)}) = (239.7 \text{ N/m}, 139.5 \text{ ms})$ . To additionally evaluate the effects of inaccurately realizing control parameters due to the uncalibrated actuator and loop delays, the effective tuned pair follows  $(g_t, \tau_t) = (\alpha_g \hat{g}_t, \hat{\tau}_t + \beta_\tau)$ , where  $(\alpha_g, \beta_\tau) = (1.04, 6 \text{ ms})$ . Before activating the tuned DR, we estimate the spectrum of the characteristic (4) using nominal values  $((m_p, k_p, c_p)$  are used here), leading to the blue squares in Fig. 3(a).

From Fig. 3(a), the rightmost root of (4) is far enough from the imaginary axis, and thus it is reasonable to assume that correcting  $\hat{u}_t$  does not induce stability issues. However, if destabilization occurs, which can be captured by the divergent system responses, a supervisory control routine should interfere, which is not considered in this work. On the other hand, the spectra of the DR subsystem (7) actuated by the desired tuned pair

$(\hat{g}_t^*, \hat{\tau}_t^*)$  and the effective one  $(g_t, \tau_t)$  are superposed as red crosses and cyan circles, respectively. Clearly, the desired pair  $(\hat{g}_t^*, \hat{\tau}_t^*)$  places the rightmost root of (7) on the imaginary axis concurring with the excitation frequency  $\omega$  for resonance, and the effective one  $(g_t, \tau_t)$  leads to spectral deviations and thus residual vibrations. The corresponding numerical responses for verification are shown in Fig. 3(b).

2) *Adaptive Correction*: Given  $\sigma_{CE} = -0.63$  in Fig. 3(a) and  $\hat{\omega} \approx 6$  Hz, the adaptive correction is executed every  $T = 7$  s as per (29) starting from  $t = 10$  s. The resulting responses  $(x_a, x_p)$  are shown in Fig. 4(a), and the root mean square of the dataset  $x_p$  over the past three cycles is depicted in Fig. 4(b), where residual vibrations are reduced each time executing the correction, before finally reaching  $|x_p| \rightarrow 0$  as expected. Accordingly, Fig. 4(c)–(i) detail the correction process. The variables  $(\sigma, \varphi)$  defined in (22) are depicted in Fig. 4(c), showing that sufficient time is required for settling  $(\sigma^{(n)}, \varphi^{(n)})$ , and  $T$  following (29) gives a good prediction. Besides,  $(\Delta \hat{k}_a^{(n)}, \Delta \hat{c}_a^{(n)})$  in Fig. 4(d) and (e) converging to zero as  $|x_p| \rightarrow 0$  concur with (15). The resulting updated nominal values  $(\hat{k}_a^{(n)}, \hat{c}_a^{(n)})$  as per (18) are depicted in Fig. 4(f) and (g), where the convergence is not achieved at the real values  $(k_a, c_a)$ , in agreement with Remark 3. Furthermore, the nominal tuned pair  $(\hat{g}_t^{(n)}, \hat{\tau}_t^{(n)})$  is corrected following Fig. 4(h) and (i), where convergence is achieved at  $(\hat{g}_t, \hat{\tau}_t) = (\hat{g}_t^*/\alpha_g, \hat{\tau}_t - \beta_\tau)$  to complement the inaccurate realization of control parameters.

At last, we point out that the recursive correction procedure is efficient so residual vibrations can be significantly reduced within three steps, which also verifies the dominance of the main terms  $(\Delta k_{a,M}, \Delta c_{a,M})$  in (27). Note that the parametric inaccuracies considered here are constant and satisfy the prerequisites outlined in Remark 2. Additional tests to show the performance of the adaptive correction when handling the time-varying inaccuracies are given in Appendix A.

*Remark 7*: According to Remark 5,  $n = 1$  corresponds to the single-step correction. One can then find from the time interval  $t \in [10 \text{ s}, 17 \text{ s}]$  in Fig. 4(a) and (b) that residual vibrations persist so the single-step correction cannot handle multiple inaccurate parameters. Similar results can also be observed in the experimental tests later and thus are not discussed.  $\square$

### B. Experimental Conditions

1) *Experimental Setup*: The main body of the experimental setup related to Fig. 1 is shown in Fig. 5(a) and (b).

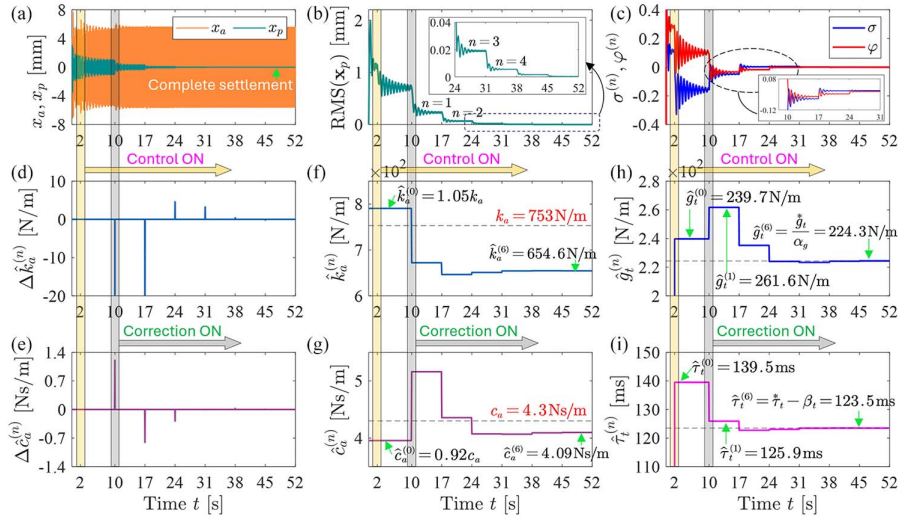


Fig. 4. Simulation tests of the adaptive correction process with  $(\omega, |f_e|) = (6 \text{ Hz}, 4 \text{ N})$ . (a) and (b) System responses. (c)–(i) Time history of the intermediate variables during the correction process. The tuned actuation force is applied from  $t = 2 \text{ s}$  and the correction with  $T = 7 \text{ s}$  is applied from  $t = 10 \text{ s}$ .

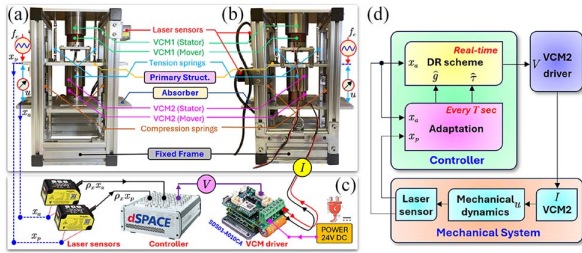


Fig. 5. Experimental setup. (a) Front view. (b) Back view. (c) Hardware loop for controlling VCM2 and monitoring  $x_p$ . (d) Data exchange among different stages when executing the adaptation.

TABLE II  
KEY PARAMETERS FOR DRIVING VCM1 AND VCM2

	$\rho_I$ [N/A]	$\rho_V$ [A/V]	$\rho_x$ [V/mm]	Stroke [mm]
VCM1	6.4	0.25	1/6	$\pm 12.5$
VCM2	8.0	0.20	1/6	$\pm 17.5$

The absolute displacements  $(x_p, x_a)$  are online monitored by two laser sensors (linearity error:  $\pm 0.2\%$ , maximum measurement error:  $0.05 \text{ mm}$ ) fixed on the frame. Through measurement and identification, the structural parameters are estimated in the first two rows of Table I. Note that no specific dampers are used and that the coupling dynamics between the absorber and the frame are the contacts between the absorber bearings and the slides fixed on frame, so  $(k_g, c_g)$  are relatively small.

To generate the excitation force  $f_e$  and the actuation force  $u$ , two voice coil motors (VCMs) are used. Each VCM is constituted by a stator (magnet) and a mover (coil). By manipulating the coil current, one can control the coupling force between the mover and the stator. Taking VCM2, used for generating  $u$ , as an example, the hardware loop is shown in Fig. 5(c).

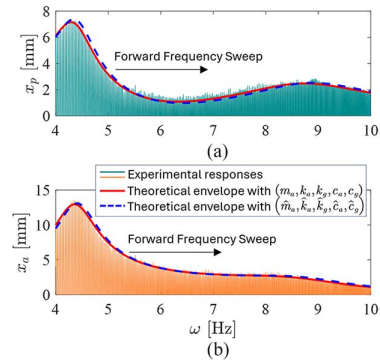


Fig. 6. Frequency sweeping test to verify the structural parameters identified in Table I and the VCM parameters in Table II.

The dSPACE MicroLabBox as the controller online processes the displacement signal  $(x_a, x_p)$  and outputs control signals in analog voltage  $V$  to the VCM driver (SDS01-A010CA). The driver then outputs current  $I$  proportional to the control signal to drive VCM2. Hence, the nominal delayed force (2) governed by  $(\hat{g}, \hat{\tau})$  is practically realized as

$$\hat{u} \rightarrow u: \begin{cases} u(t) = \rho_I I(t - \tau_I) \\ I(t) = \rho_V V(t - \tau_V) \\ V(t) = \hat{\eta} \rho_x \hat{g} x_a(t - \hat{\tau}) \end{cases} \quad (33)$$

where  $(\rho_I, \rho_V, \rho_x)$  are three conversion coefficients performed in VCM2, in VCM driver, and in laser sensors, respectively;  $\hat{\eta} = (\hat{\rho}_x \hat{\rho}_I \hat{\rho}_V)^{-1}$  is a conversion coefficient customized as per the nominal values of  $(\rho_I, \rho_V, \rho_x)$  and is performed in the controller;  $(\tau_I, \tau_V)$  are two inherent delays related to the tracking performance of the driver and the VCM. Fig. 5(d) shows the relationship of (33) and the data exchange among different sections when executing the adaptation as per Fig. 2.

2) *Inaccurate Realization of Control Parameters:* From (33), the actual gain output  $g$  depends on the knowledge of

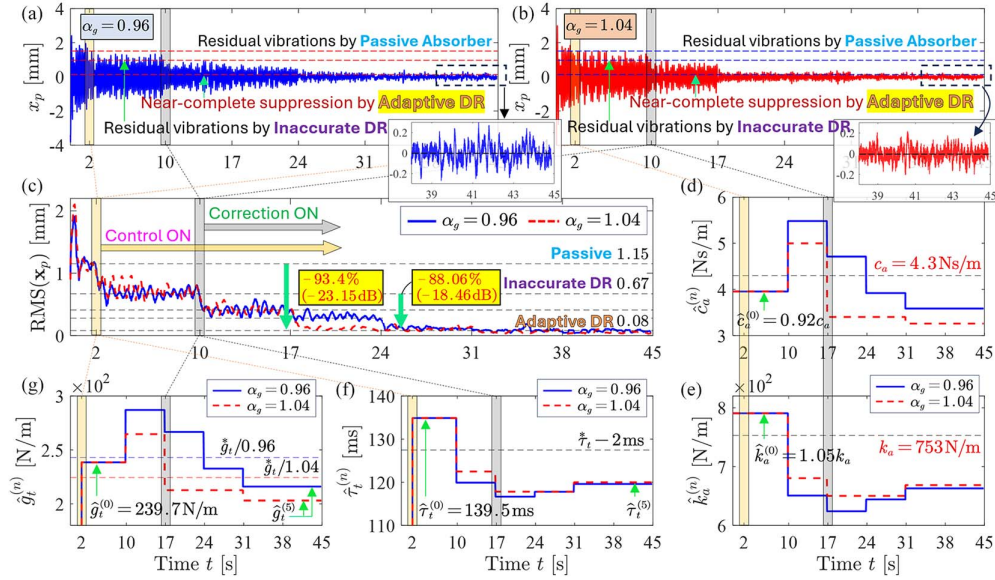


**Fig. 7.** Experimental tests of the adaptive DR with  $(\omega, |f_e|, T) = (6 \text{ Hz}, 4 \text{ N}, 7 \text{ s})$ . (a) and (b) Responses  $x_p$  when experimentally testing the adaptive correction for  $\alpha_g = [0.96, 1.04]$  and  $\hat{\tau}_t = \hat{\tau}_t + 2 \text{ ms}$ . (c) Evaluation of (a) and (b) by the root square root of the last three cycles of  $x_p$ . (d)–(g) Parametric variations in the correction process. The tuned actuation force is applied from  $t = 2 \text{ s}$  and the adaptive correction is applied from  $t = 10 \text{ s}$ .

$(\rho_I, \rho_V, \rho_x)$ , and the actual delay  $\tau$  is affected by  $(\tau_I, \tau_V)$ . More specifically, one has

$$(\hat{g}, \hat{\tau}) \rightarrow (g, \tau) : \begin{cases} g = \hat{\eta} \rho_x \rho_V \rho_I \hat{g} = \frac{\rho_x \rho_V \rho_I}{\hat{\rho}_x \hat{\rho}_V \hat{\rho}_I} \hat{g} \\ \tau = \hat{\tau} + \tau_I + \tau_V. \end{cases} \quad (34)$$

When actually realizing  $\hat{g}$ ,  $\rho_V$  is user-defined as per the rated current of the VCM,  $\rho_x$  is inherent in the laser sensor, and  $\rho_I$  signifies the thrust constant (electromagnetic coupling coefficient) of the VCM. In practice,  $(\hat{\rho}_V, \hat{\rho}_x)$  can be accurately known, so  $(\hat{\rho}_V, \hat{\rho}_x) = (\rho_V, \rho_x)$ . However,  $\rho_I$  usually needs to be calibrated or identified before use to specify  $\hat{\eta}$  in the controller, and the inaccuracy  $\hat{\rho}_I \neq \rho_I$  leads to  $g \neq \hat{g}$ . The key parameters for driving the two VCMs are listed in Table II. Similarly, we have  $\tau \neq \hat{\tau}$  for realizing the delay  $\hat{\tau}$  due to the loop delays  $(\tau_I, \tau_V)$ .

For a linear system, the relationship between  $(\hat{g}, \hat{\tau})$  and  $(g, \tau)$  as (34) should be fixed or slightly fluctuate around constant levels, as aforementioned in Remark 1. With the adaptive correction method,  $(\rho_I, \rho_V, \rho_x)$  and  $(\tau_I, \tau_V)$  for VCM2 in addition to  $(\omega, m_a, k_a, k_g, c_a, c_g)$  all do not need to be exactly identified for tuning the DR to achieve complete vibration suppression, which can help significantly reduce the complexities and enhance the robustness for practically deploying the DR.

### C. Experiment Verifications

1) *Parametric Test:* We start with testing the effectiveness of the parameters identified in Tables I and II using a frequency sweeping test. Given the operational space of the setup and the VCM performance, the excitation of  $|f_e| = 2.8 \text{ N}$  sweeps from 4 Hz to 10 Hz, with a sufficiently low sweeping rate adopted to reduce the interferences at adjacent frequencies. As per Table II, it corresponds to the amplitude  $|V^{[1]}| = |f_e| / (\rho_I^{[1]} \rho_V^{[1]}) = 1.75 \text{ V}$  ( $(\cdot)^{[1]}$  denotes VCM1) of the control

signal in analog voltage to drive VCM1. The results are shown in Fig. 6, where theoretical results are obtained by solving (1).

The red solid curves in Fig. 6 correspond to theoretical envelopes based on real values  $(m_a, k_a, k_g, c_a, c_g)$ , and the blue dashed curves correspond to nominal values  $(\hat{m}_a, \hat{k}_a, \hat{k}_g, \hat{c}_a, \hat{c}_g)$ . Clearly, the real values better predict experimental responses. Note that even if we use such real values, which are obtained by fitting the envelopes of experimental responses, a small mismatch still appears within  $\omega \in [5, 8] \text{ Hz}$ . That is, system dynamics predicted by a constant parameter composition can fail within a specific frequency band, which is also the case for tuning the DR to achieve complete vibration suppression. This again indicates the necessity of developing a general adaptation method to reduce the reliance on exact system modeling.

2) *Adaptive Correction:* Following Fig. 4, the experimental tests are performed under  $(\omega, |f_e|) = (6 \text{ Hz}, 4 \text{ N})$ , and nominal values  $(\hat{m}_a, \hat{k}_a, \hat{k}_g, \hat{c}_a, \hat{c}_g)$  in Table I with  $\hat{\omega} = 0.98\omega$  are used for tuning the DR. Additionally, we consider two cases where  $\hat{g}_t$  is deviated by either +4% ( $\alpha_g = 1.04$ ) or -4% ( $\alpha_g = 0.96$ ), which can be achieved by manipulating  $\hat{\eta}$  in (33), to mimic the cases where  $\rho_I$  of VCM2 is inaccurately estimated. Given that the two inevitable loop delays  $(\tau_I, \tau_V)$  in (33) can be small, the output of  $\hat{\tau}_t$  follows  $\hat{\tau}_t + 2 \text{ ms}$  to increase deviations while not amplifying vibrations in the passive case, i.e., to satisfy (31). The correction is still performed every  $T = 7 \text{ s}$  once activated. The experimental results are in Fig. 7.

From the time interval  $t \in [2 \text{ s}, 10 \text{ s}]$  of Fig. 7(a) and (b), the inaccurately tuned DR suppresses vibrations in the passive case while residual vibrations appear as expected. Once the adaptive correction is activated, residual vibrations are significantly suppressed within three correction steps. The root mean squares dynamically calculated following the last three cycles of  $x_p$

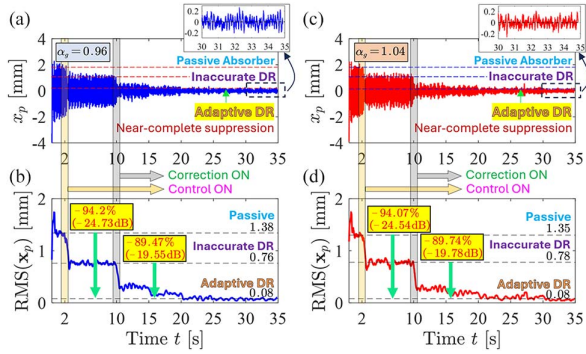


Fig. 8. Experimental tests of the adaptive DR at  $(\omega, |f_e|) = (7 \text{ Hz}, 4 \text{ N})$  with  $T = 5 \text{ s}$ . (a) and (b) Case  $\alpha_g = 0.96$ . (c) and (d) Case  $\alpha_g = 1.04$ . The tuned actuation force is applied from  $t = 2 \text{ s}$  and the adaptive correction is applied from  $t = 10 \text{ s}$ . Parameters of the inaccurate DR follow Fig. 7.

shown in Fig. 7(c) depict the enhanced performance. The adaptive DR reduces the residual vibration by 88.06% ( $-18.46 \text{ dB}$ ). Compared with the passive absorber within  $t \in [0, 2 \text{ s}]$ , the vibration is finally suppressed by up to 93.4% ( $-23.15 \text{ dB}$ ). Note that this percentage number is rather high since the test frequency  $\omega = 6 \text{ Hz}$  is around the natural frequency of the absorber, see also the antiresonance peak in Fig. 6(a). Besides, in this process,  $\text{rms}(x_p) = 0.08 \text{ mm}$  is set as the lower threshold value  $\delta_{\text{low}}$  of activating the correction as per (32) to reduce the risks of correction deviations given the increasing noise effects in  $x_p$ .

Fig. 7(d) and (e) details the parametric variations during the correction process. Different from Fig. 4(h) and (i), the final convergences at  $(\hat{g}_t^{(5)}, \hat{\tau}_t^{(5)})$ , as shown in Fig. 7(g) and (f), do not match  $(\hat{g}_t^*/\alpha_g, \hat{\tau}_t^* - 2 \text{ ms})$  since inaccuracies exist in the identified  $(m_a, k_a, k_g, c_a, c_g)$  and since the ideal complete vibration suppression  $|x_p| \equiv 0$  is not achieved at last. However, one should notice that  $\hat{g}_t^{(5)}$  when  $\alpha_g = 0.96$  is larger than that when  $\alpha_g = 1.04$ , which is desired to complement the scaled gain deviations in the two cases. On the other hand,  $\hat{\tau}_t^{(5)}$  in the two cases tend to converge to the same value since the delay deviations in the two cases are the same.

At last, to show the generality nature of the adaptation method, an additional test is performed at  $\omega = 7 \text{ Hz}$  following the same procedure of Fig. 7 except for changing  $T$  to  $T = 5 \text{ s}$  based on the spectral analysis similar to Fig. 4(a) and maintaining the inaccurate deviations of other nominal parameters. The resulting responses  $x_p$  are shown in Fig. 8. One can see that the adaptation correction is still effective and efficient so that residual vibrations resulting from the inaccurate DR can be suppressed by more than 89% within four steps, finally yielding up to 94% vibration reduction compared with the passive absorber.

## VI. CONCLUSION

This work aims to eliminate the residual vibrations caused by an inaccurately tuned DR arising from the inaccurate knowledge of the parameters needed to calculate the nominal values of the tuned pair  $(\hat{g}_t, \hat{\tau}_t)$  in the controller, including all structural

parameters of the absorber,  $(\hat{m}_a, \hat{k}_a, \hat{k}_g, \hat{c}_a, \hat{c}_g)$ , the vibration frequency,  $\hat{\omega}$ , and the relationship between the effective  $(g, \tau)$  and nominal  $(\hat{g}, \hat{\tau})$  control parameters. To this end, an online recursive adaptive correction strategy is proposed by equating the effects of the inaccurately tuned actuation force  $u_t$  to the inappropriate alteration of  $(\hat{k}_a, \hat{c}_a)$ . Based on the equivalent model, the resulting adaptive DR can directly correct  $(\hat{g}_t, \hat{\tau}_t)$  as per real-time system responses without needing to identify the real values of all parameters involved in force tuning, thus simplifying implementation.

The effectiveness and efficiency of the adaptive DR are both numerically and experimentally validated. Simulations show that residual vibrations by an inaccurately tuned DR can be significant. Alternatively, the adaptive DR can theoretically eliminate the residual vibration and reach convergence within very limited correction steps. In experiments, residual vibrations caused by the inaccurately tuned DR can be suppressed by over 88%, finally settling the primary by up to 93.4% compared with the passive case, even if the test frequency is around the absorber's natural frequency. Besides, the mechanism of the inaccurate realization  $(\hat{g}, \hat{\tau})$  in practice is discussed.

Generalizing from the previous work [32], which focuses on the inaccuracies in  $(\hat{k}_a, \hat{c}_a)$ , the adaptive DR can now be more easily deployed to maximize its capacity for complete vibration suppression thanks to the reduced accuracy requirements on parameter identification and the stronger robustness against parametric variations. Our future work would address MDOF absorbers, which have been recently demonstrated to offer significant advantages in specific scenarios [19], [20], [21]. Besides, more specific conditions are needed to guide the design of  $\delta_{\text{up}}$  in (31), and a more general adaptation method capable of handling time-varying parametric inaccuracies beyond the prerequisites in Remark 2 is also worthy of investigation.

## APPENDIX A LIMITATIONS WHEN HANDLING TIME-VARYING PARAMETRIC INACCURACIES

We here test the limitations of the recursive adaptive correction when the parametric inaccuracies are time-varying. For demonstration, we consider a time-varying frequency  $\omega$ . Based on the test conditions in Fig. 4, we first let  $\omega$  increase at the rate of  $+0.015 \text{ Hz/s}$  from  $6 \text{ Hz}$  during  $t \in [10, 52] \text{ s}$ . To mimic a possible practical case where such frequency variations are not detected due to a poor sensor or calculation errors, the nominal frequency  $\hat{\omega} = 0.98 \times 6 \text{ Hz}$  is fixed in the controller. The variations of  $\omega$  and the resulting system responses in simulation are shown in Fig. 9(a).

From the interval  $t \in [10, 31] \text{ s}$  in Fig. 9(a), each execution of the correction with  $T = 7 \text{ s}$  can confine residual vibrations. However, the vibration suppression is far from complete even after multiple steps since the correction is transfer function-based as per (15). More specifically, the steady-state data of  $(x_a, x_p)$  are required when constructing (22) to ensure accuracy since a transfer function evaluated with  $s = j\omega_g$  governs steady-state responses, while such data are unavailable here due to the time-varying  $\omega$ , as also mentioned in the definition of (29). On the other hand, since the vibration can be effectively controlled

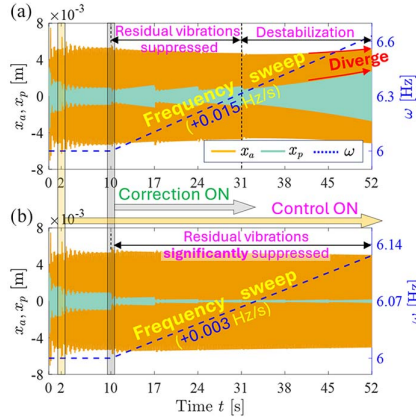


Fig. 9. Simulation test of the recursive adaptive correction with time-varying frequencies, with  $\omega$  linearly increasing from 6 Hz during  $t \in [10, 52]$  s. (a) Sweeping rate is +0.015 Hz/s. (b) Sweeping rate is +0.003 Hz/s. Remaining test conditions are identical to those specified in Fig. 4.

by and large as  $\omega$  varies, we can naturally infer that the residual vibrations can be theoretically eliminated if  $\omega$  varies more slowly than a complete correction process, or the varying rate of  $\omega$  during the correction process is sufficiently low to yield a negligible transient process. To test the latter condition, we reduce the frequency-sweeping rate to +0.003 Hz/s (the lower the smaller residual vibrations), thus yielding Fig. 9(b). In this case, the residual vibrations can be suppressed to a sufficiently low level, see also the frequency response prediction in Fig. 6. The above analysis again verifies the prerequisite of the adaptive correction given in Remark 2.

Particularly, we add that even with a good estimation of  $\omega$  when starting the correction and if  $\omega$  varies sufficiently slowly, frequency detection is still required since the stability estimation and the selection of  $T$  as done in Fig. 3(a) may lose effectiveness due to the increased mismatch between  $\hat{\omega}$  and  $\omega$ , as verified by the destabilization that occurs when  $t > 31$  s in Fig. 9(a). The above conclusions also apply to the case where  $(m_a, k_a, c_a, c_q, g, \tau)$  are time-varying, albeit slowly. The SIMULINK-based simulation model and results corresponding to Fig. 9 are given in Appendix C.

## APPENDIX B

### APPLICABILITY OF THE ADAPTIVE CORRECTION FOR MDOF PRIMARY STRUCTURES

The primary structure may have internal degrees of freedom in practical applications. We here show that the generalized adaptive correction procedure proposed in Fig. 2 can still be applicable under specific conditions. We consider a 2DOF primary structure for demonstration, leading to Fig. 10, where  $(m_q, c_q, k_q)$  are newly introduced compared to Fig. 1.

System dynamics are now 3DOF and are governed by

$$\begin{cases} m_a \ddot{x}_a + c_g \dot{x}_a + k_g x_a + c_a (\dot{x}_a - \dot{x}_p) + k_a (x_a - x_p) = u \\ m_p \ddot{x}_p + c_p \dot{x}_p + k_p x_p + c_a (\dot{x}_p - \dot{x}_a) + k_a (x_p - x_a) \\ + c_q (\dot{x}_p - \dot{x}_q) + k_q (x_p - x_q) = f_e - u \\ m_q \ddot{x}_q + c_q (\dot{x}_q - \dot{x}_p) + k_q (x_q - x_p) = 0. \end{cases} \quad (35)$$

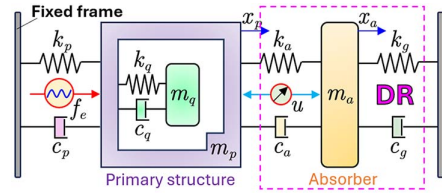


Fig. 10. Possible operating mode where the primary structure has an internal degree of freedom.

Note that the first equation of (35) is identical to that of (1), so the tuning mechanism (8) still holds without modifications. This is a natural result of the fact that the dynamics of  $m_q$  take no effect when  $|x_p| \equiv 0$ , i.e.,  $x_p$  is essentially the excitation of  $m_q$ . On the other hand, revisiting (9) and (15), the adaptive correction needs to construct the transfer function from  $x_a$  to  $x_p$ , which is still determined by the first equation of (35), where the dynamics of  $m_q$  take no effect. This aligns with the fact that the inherent dynamics of the primary structure do not affect the force transmission relationship between  $m_a$  and  $m_p$ . Hence, compared to Fig. 1, no modifications to the correction calculations are required either when handling the present 2DOF primary structure. The only parameter being affected is the time gap  $T$  between the two consecutive correction steps. As per (29), the lower bound of  $T$  depends on the settling time  $t_s$  and thus the spectrum of the characteristic equation.

We consider  $(m_q, c_q, k_q) = (0.4 \text{ kg}, 2 \text{ Ns/m}, 900 \text{ N/m})$  for verifications. The test conditions, including the settings of the remaining structural parameters, the excitation, and the parametric inaccuracies (nominal tuned pair  $(\hat{g}_t^{(0)}, \hat{\tau}_t^{(0)})$ ) follow those in Section V-A. Similar to Fig. 3, the real part of the rightmost characteristic roots can be obtained as  $\sigma_{CE} = -1.33$  (the characteristic equation related to (35) is omitted), so we let  $T = 5$  s. The simulation results are given in Fig. 11.

Comparing Figs. 4 and 11, one can see from the time interval  $t \in [2, 10]$  s that the additional structure  $m_q$  inherent in  $m_p$  can amplify the residual vibrations caused by the inaccurately tuned DR (with the same nominal tuned pair) so that the vibration level can unfavorably exceed that in the passive case (i.e.,  $t < 2$  s). Even so, it does not affect the efficacy of the adaptive DR, which eliminates the residual vibration (99% reduction) within three steps since the activation at  $t = 10$  s.

Based on the above, one can conclude that increasing the number of the substructures inherent in  $m_p$ , i.e., the primary structure has multiple internal degrees of freedom, does not affect the direct applicability of the correction procedure following Fig. 2 to achieve complete vibration suppression, as long as the tuning mechanism (8) and the transfer function (9) are still effective. This test with an MDOF primary structure also signifies possible wider applications of the DR technique, which is less-reported in the open literature. The used SIMULINK-based simulation model and results corresponding to Fig. 11 are provided in Appendix C.

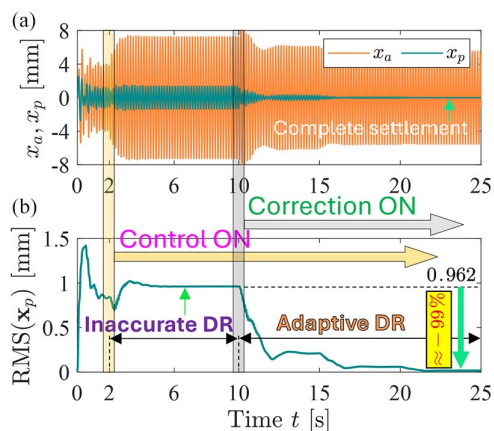


Fig. 11. Simulation test of the adaptive correction with a 2DOF primary structure as Fig. 10, where  $(m_q, c_q, k_q) = (0.4 \text{ kg}, 2 \text{ Ns/m}, 900 \text{ N/m})$ . (a) Time history of the system responses. (b) Dynamical evaluations of the rms of  $x_p$ . The tuned actuation force is applied from  $t = 2 \text{ s}$  and the adaptive correction with  $T = 5 \text{ s}$  is applied from  $t = 10 \text{ s}$ .

### APPENDIX C OPEN-SOURCE MATERIALS

The SIMULINK-based simulation models and results related to Figs. 4, 9, and 11, as well as the video recordings of the experiments related to Figs. 7 and 8 are available at <https://bit.ly/4nJOVDY>.

### REFERENCES

- [1] N. Olgac and B. Holm-Hansen, "A novel active vibration absorption technique: Delayed resonator," *J. Sound Vib.*, vol. 176, no. 1, pp. 93–104, 1994.
- [2] H. Elmali, M. Renzulli, and N. Olgac, "Experimental comparison of delayed resonator and pd controlled vibration absorbers using electromagnetic actuators," *J. Dyn. Sys., Meas., Control*, vol. 122, no. 3, pp. 514–520, 2000.
- [3] D. Filipovic and N. Olgac, "Torsional delayed resonator with velocity feedback," *IEEE/ASME Trans. Mechatronics*, vol. 3, no. 1, pp. 67–72, Mar. 1998.
- [4] T. Vyhřídál, N. Olgac, and V. Kučera, "Delayed resonator with acceleration feedback—complete stability analysis by spectral methods and vibration absorber design," *J. Sound Vib.*, vol. 333, no. 25, pp. 6781–6795, 2014.
- [5] N. Olgac, "Delayed resonators as active dynamic absorbers," U.S. Patent 5431261, 1995.
- [6] Y. Sun and J. Xu, "Experiments and analysis for a controlled mechanical absorber considering delay effect," *J. Sound Vib.*, vol. 339, pp. 25–37, 2015.
- [7] X. Zhang, J. Xu, and J. Ji, "Modelling and tuning for a time-delayed vibration absorber with friction," *J. Sound Vib.*, vol. 424, pp. 137–157, 2018.
- [8] D. Pilbauer, T. Vyhřídál, and N. Olgac, "Delayed resonator with distributed delay in acceleration feedback—Design and experimental verification," *IEEE/ASME Trans. Mechatronics*, vol. 21, no. 4, pp. 2120–2131, Aug. 2016.
- [9] V. Kučera, D. Pilbauer, T. Vyhřídál, and N. Olgac, "Extended delayed resonators—design and experimental verification," *Mechatronics*, vol. 41, pp. 29–44, 2017.
- [10] Y. Liu, N. Olgac, and L. Cheng, "Delayed resonator with multiple distributed delays—considering and optimizing the inherent loop delay," *J. Sound Vib.*, vol. 576, 2024, Art. no. 118290.
- [11] O. Eris, B. Alikoc, and A. F. Ergenc, "A new delayed resonator design approach for extended operable frequency range," *J. Vib. Acoust.*, vol. 140, no. 4, 2018, Art. no. 041003.
- [12] G. Yan, M. Fang, and J. Xu, "Analysis and experiment of time-delayed optimal control for vehicle suspension system," *J. Sound Vib.*, vol. 446, pp. 144–158, 2019.
- [13] K. Wu et al., "Experimental research on vehicle active suspension based on time-delay control," *Int. J. Control*, vol. 97, no. 5, pp. 1157–1173, 2024.
- [14] F. Wang, X. Sun, H. Meng, and J. Xu, "Time-delayed feedback control design and its application for vibration absorption," *IEEE Trans. Ind. Electron.*, vol. 68, no. 9, pp. 8593–8602, Sep. 2021.
- [15] S. Mohanty and S. Dwivedy, "Linear and nonlinear analysis of traditional and non-traditional piezoelectric vibration absorber with time delay feedback for simultaneous resonance conditions," *Mech. Syst. Sig. Process.*, vol. 161, 2021, Art. no. 107980.
- [16] Y. Liu and L. Cheng, "A high-static-low-dynamic-stiffness delayed resonator vibration absorber," *Commun. Nonlinear Sci. Numer. Simul.*, vol. 140, 2025, Art. no. 108299.
- [17] T. Vyhřídál, D. Pilbauer, B. Alikoc, and W. Michiels, "Analysis and design aspects of delayed resonator absorber with position, velocity or acceleration feedback," *J. Sound Vib.*, vol. 459, 2019, Art. no. 114831.
- [18] J. Cai, Q. Gao, Y. Liu, and N. Olgac, "Control design, analysis, and optimization of fractional-order delayed resonator for complete vibration absorption," *J. Sound Vib.*, vol. 571, 2024, Art. no. 118083.
- [19] N. Olgac and R. Jenkins, "Actively tuned noncollocated vibration absorption: An unexplored venue in vibration science and a benchmark problem," *IEEE Trans. Control Syst. Technol.*, vol. 29, no. 1, pp. 294–304, Jan. 2021.
- [20] H. Silm, M. Kuře, J. Bušek, W. Michiels, and T. Vyhřídál, "Spectral design and experimental validation of noncollocated vibration suppression by a delayed resonator and time-delay controller," *IEEE Trans. Control Syst. Technol.*, vol. 32, no. 1, pp. 73–85, Jan. 2024.
- [21] T. Vyhřídál, W. Michiels, Z. Neusser, J. Bušek, and Z. Šika, "Analysis and optimized design of an actively controlled two-dimensional delayed resonator," *Mech. Syst. Sig. Process.*, vol. 178, 2022, Art. no. 109195.
- [22] Z. Šika, J. Krivošej, and T. Vyhřídál, "Three dimensional delayed resonator of Stewart platform type for entire absorption of fully spatial vibration," *J. Sound Vib.*, 2024, Art. no. 118154.
- [23] X. Mao and W. Ding, "Nonlinear dynamics and optimization of a vibration reduction system with time delay," *Commun. Nonlinear Sci. Numer. Simul.*, vol. 122, 2023, Art. no. 107220.
- [24] J. Peng, Y. Li, S. Lenci, X. Yang, and L. Wang, "Vibration suppression of suspended cables with three-to-one internal resonances via time-delay feedback," *Eur. J. Mechanics-A/Solids*, vol. 109, 2025, Art. no. 105487.
- [25] B. Yan, X. Wang, H. Ma, W. Lu, and Q. Li, "Hybrid time-delayed feedforward and feedback control of lever-type quasi-zero-stiffness vibration isolators," *IEEE Trans. Ind. Electron.*, vol. 71, no. 3, pp. 2810–2819, Mar. 2024.
- [26] J. Cai, Q. Gao, and S. Zhu, "Experimental investigation of time-delayed control for enhanced performance in a high-static-low-dynamic-stiffness vibration isolation system," *IEEE/ASME Trans. Mechatronics*, vol. 424, pp. 1–12, 2024.
- [27] D. Pilbauer, T. Vyhřídál, and W. Michiels, "Optimized design of robust resonator with distributed time-delay," *J. Sound Vib.*, vol. 443, pp. 576–590, 2019.
- [28] M. Kuře, J. Bušek, I. Boussaada, W. Michiels, S.-I. Niculescu, and T. Vyhřídál, "Robust delayed resonator with acceleration feedback—Design by double root assignment and experimental validation," *J. Sound Vib.*, vol. 576, 2024, Art. no. 118261.
- [29] Y. Liu, B. Yan, and L. Cheng, "Delayed resonator with hybrid multiple-delayed control for enhanced complete vibration suppression," *IEEE/ASME Trans. Mechatronics*, early access, 2025.
- [30] Y. Liu, J. Cai, N. Olgac, and Q. Gao, "A robust delayed resonator construction using amplifying mechanism," *J. Vib. Acoust.*, vol. 145, no. 1, 2023, Art. no. 011010.
- [31] M. E. Renzulli, R. Ghosh-Roy, and N. Olgac, "Robust control of the delayed resonator vibration absorber," *IEEE Trans. Control Syst. Technol.*, vol. 7, no. 6, pp. 683–691, Nov. 1999.
- [32] M. Hosek and N. Olgac, "A single-step automatic tuning algorithm for the delayed resonator vibration absorber," *IEEE/ASME Trans. Mechatronics*, vol. 7, no. 2, pp. 245–255, Jun. 2002.
- [33] T. Vyhřídál and P. Zitek, "Mapping based algorithm for large-scale computation of quasi-polynomial zeros," *IEEE Trans. Autom. Control*, vol. 54, no. 1, pp. 171–177, Jan. 2009.